EFFECTS OF GEOMETRICAL NONLINEARITIES ON ELASTIC-PLASTIC BEHAVIOR OF REINFORCED CONCRETE SLABS

Youichi MINAKAWA

(Received May 31, 1985)

Summary

Four analyzing methods incorporating two concrete models and the finite element method with and without finite deformations are adopted. They make clear the influence of geometrical nonlinearities on the elastic-plastic behavior of reinforced concrete slabs.

1 Introduction

Evaluating ultimate loads of reinforced concrete slabs, Johansen theory gives considerably small values compared with values obtained by experiments. It is well-known that the difference is caused by compressive membrane stresses which occur in slabs according as the spreading of cracks.

The finite element method is one of the most convenient analyzing method for reinforced concrete structures. In order to analyze reinforced concrete slabs, two finite element models are presented, one uses modified stiffness and the other uses the layered element. Layered models have met with success to get elastic-plastic behavior of slabs and shells.

Wanchoo et al [4] adopted an element without inplane freedom and get a good match result for a corner supported slabs. Hand et al [3] adopted an element with inplane freedom and indicated that inplane supporting conditions influenced the stiffness of the corner supported slab.

Idealizations of concrete are also essential to apply the finite element method to reinforced concrete slabs. Dobashi and Ueda [21] adopted a combined use of finite element models with and without inplane freedom, and the concrete models proposed by Kupher et al [1] and constructed by yield potential functions, and showed that for slabs without inplane constraint both finite element models gave similar results, but for slabs with inplane constraint 1. the finite element model without inplane freedom gave much smaller ultimate load than the element with inplane freedom ; 1. a concrete model expressed with perfect elastic-plastic curves gave larger ultimate load than a model considering stress reduction after maximum compressive stress ; 1. the latter model gave a match results with experiments.

This paper examines effects of gemetrical nonlinearities on elastic-plastic behavior of reinforced concrete slabs, because it seems that the large inplane compressive stress make stimulate the nonlinearities. Adopting two concrete models and a 18-degree-of-freedom shallow shell layered triangular element, and basing on two analytical assumptions, one includes the finite deformations and the other assumes the infinitesimal deformations, we analyze some concrete slabs of which experimental load-deflection curves were reported.

2 Material Properties

2 — 1 Concrete

Many models for biaxial concrete are used to construct constitutional equations. Noguchi[20] examined applicabilities of typical concrete models until peak stresses. It is necessary to idealize concrete behavior after peak stresses, when we seek ultimate loads of structures where concrete may be failed by compressive stresses. Here, we adopt 2 concrete models where stress reductions after peak stress are included.

a) Concrete Model A

It is a model that is constructed by a rule in which computed strains are never modified, because we apply the finite element method of a displacement method. Except biaxial concrete failure regions idealized uniaxial stress-strain curves of concrete are introduced in principal strain directions. Biaxial concrete failures are evaluated by the octahedral shear stress.

(i) Stress-Strain curves

Uniaxial stress-strain curves are idealized with three brocken lines shown in Fig. 1, where

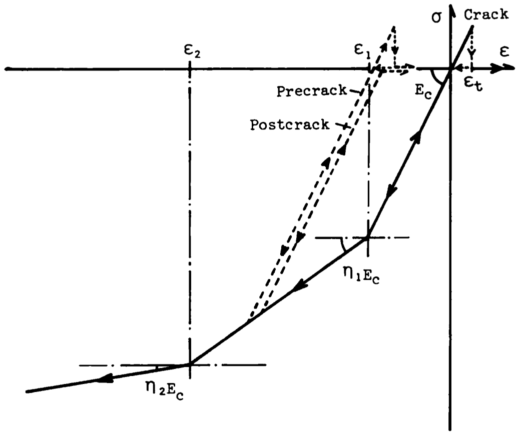

Fig. 1 Uniaxial Stress-strain for Concrete Model A

unloading are included. Subelement concretes in each element are assumed as orthotropic material, where material axes coincide with the principal strain axes before cracking. Once cracks have formed, material axes coincide with the principal strain axes when first cracks open. Determine E_1 and E_2 for material axes from uniaxial curves, we form stree-strain matrix

$$[D_{12}^*]=\frac{1}{1-\nu^2}\begin{bmatrix} E_1 & \nu\sqrt{E_1E_2} & 0 \\ & E_2 & 0 \\ \mathrm{sym} & & (1-\nu)\sqrt{E_1E_2}/2 \end{bmatrix} \qquad (1)$$

The expression (1) is proposed by Isohata.[14]

(ii) Criteria for Biaxial Failure and Stress Reductions

Concrete failures in biaxial compressions are evaluated by the criteria of octahedral shear stress, which is given by

$$f_{oct}=\sqrt{(\sigma_1-\sigma_2)^2+(\sigma_2-\sigma_3)^2+(\sigma_3-\sigma_1)^2}/3-\{c+n(\sigma_1+\sigma_2+\sigma_3)/3\}\geqq 0 \tag{2}$$

where constants c, n are defined to satisfy the conditions at uniaxial tests $\sigma_2=\sigma_3=0$, $\sigma_1=f_c'(<0)$ and biaxial tests $\sigma_3=0$, $\sigma_1=\sigma_2=df_c'$ ($d=1.16$ reported by Kupfer[1]). Then, we have

$$f_{oct}=\sqrt{2}(\sqrt{\sigma_1{}^2+\sigma_2{}^2-\sigma_1\sigma_2}+0.1212(\sigma_1+\sigma_2)+0.8788f_c')/3 \tag{3}$$

where f_c' means uniaxial compressive strength of concrete.

After the principal strain in subelement in each concrete element reaches to ε_{cu}, which is the strain at f_c', the stress in the principal direction is reduced by

$$\begin{cases} \Delta\sigma_i=-0.24E_c(\varepsilon_i-\varepsilon_{cu})\geqq 0 & (4\varepsilon_{cu}\leqq\varepsilon_i\leqq\varepsilon_{cu}) \\ \sigma_i=0 & (\varepsilon_i<4\varepsilon_{cu}) \end{cases} \tag{4}$$

Biaxial strength envelopes and stress reductions of concrete model A are depicted in Figs. 2 and 3, respectively. Tangent stiffness to the perpendicular direction of cracks and to both principal directions after concrete failures are assumed zero.

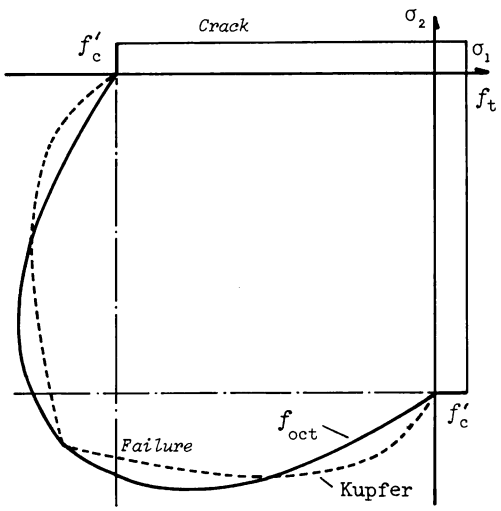

Fig. 2 Biaxial Strength for Concrete Model A

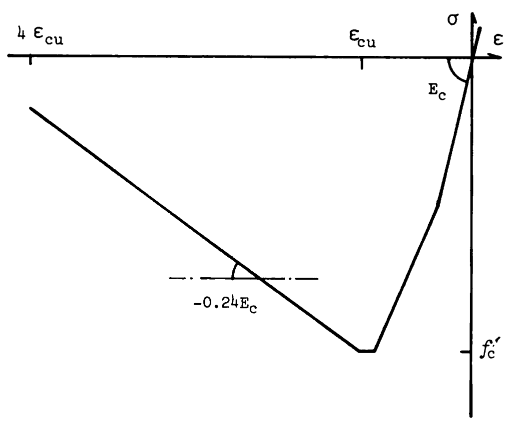

Fig. 3 Stress Reduction for Concrete A

b) Concrete Model B

Darwin and Pecknold[7] proposed a biaxial concrete model constructed by the concept of "equivalent uniaxial strain". Examining typical biaxial concrete models until peak stresses, Noguchi[20] reported that the model gives the best results in the both principal directions. But, Dobashi et al[21] showed that the Darwin's model have an improper evaluation of maximum compressive stress in tension-compression regions, and presented another evaluating expression. Then, we introduce an uniaxial concrete model to treat compressive strength of concrete for the regions.

(i) Tangent Stiffness in Principal Directions

The equivalent uniaxial strain increments for nonlinear material are defined by

$$\Delta\varepsilon_{iu}=\Delta\sigma_i/E_i \tag{5}$$

Using the strain increments, we define equivalent uniaxial strains in principal stress dirctions

$$\varepsilon_{1u}=\Sigma(\Delta\varepsilon_{1u}-\nu\sqrt{E_2/E_1}\Delta\varepsilon_{2u})$$
$$\varepsilon_{2u}=\Sigma(\Delta\varepsilon_{2u}-\nu\sqrt{E_1/E_2}\Delta\varepsilon_{1u}) \tag{6}$$

where when argument angle changes more than $\pi/4$ from their initial directions, we interchange $\Delta\varepsilon_{1u}$ with $\Delta\varepsilon_{2u}$. Here we employ Eq. (6) including effects of Poisson's ratio ν. In the expression proposed by Darwin[7], the Poisson's ratio term are neglected.

In tension regions, concrete is assumed by an elastic brittle material. Denoting initial tangential stiffness for the model E_0, tangential stiffness for the principal axis for compression is given by

$$E_i=\frac{d\sigma_i}{d\varepsilon_{iu}}=\frac{(1+\varepsilon_{iu}/\varepsilon_{ic})(1-\varepsilon_{iu}/\varepsilon_{ic})}{1+(E_0/E_{ic}-2)\varepsilon_{iu}/\varepsilon_{ic}+(\varepsilon_{iu}/\varepsilon_{ic})^2}E_0\geqq 0 \tag{7}$$

where $E_{ic}=\sigma_{ic}/\varepsilon_{ic}$, $E_0/E_{ic}\geqq 2$, and σ_{ic} and ε_{ic} are determined by the following procedure.
Compression-Compression regions ; Expressing principal stress ratio $\alpha\,(\alpha=\sigma_1/\sigma_2$ where $\sigma_2\leqq\sigma_1)$, maximum compressive stresses are determined by the criteria proposed by Kupfer[1]

$$\sigma_{2c}=\frac{1+3.65\alpha}{(1+\alpha)^2}f_c', \quad \sigma_{1c}=\alpha\sigma_{2c} \tag{8}$$

Equivalent uniaxial strains ε_{ic} at which concrete takes maximum stresses are evaluated by

$$\varepsilon_{ic}=\varepsilon_{cu}(3.15\sigma_{ic}/f_c'-2.15) \quad \text{for} \quad |\sigma_{ic}|\geqq|f_c'|$$
$$\varepsilon_{ic}=\varepsilon_{cu}(-1.6(\sigma_{ic}/f_c')^2+2.25(\sigma_{ic}/f_c')+0.35)(\sigma_{ic}/f_c') \quad \text{for} \quad |\sigma_{ic}|<|f_c'| \tag{9}$$

Tension-Compression regions ; Tensive strength of concrete is evaluated by

$$\sigma_{1t}=(1-0.8\sigma_2/f_c')f_t' \tag{10}$$

where f_t' means uniaxial tensive strenght, which is proposed by Kupfer[1]. Setting $\alpha=0$ in Eq. (8), the expression lets evaluate maximum uniaxial compressive strenght of concrete.

Then, using tangent stiffness E_1 and E_2, we define the stress-strain matrix for this model

$$[D_{12}^*]=\frac{1}{1-\nu^2}\begin{bmatrix} E_1 & \nu\sqrt{E_1E_2} & 0 \\ & E_2 & 0 \\ \text{sym} & & (E_1+E_2-2\nu\sqrt{E_1E_2})/4 \end{bmatrix} \tag{11}$$

where Poisson's ratio $\nu=0.2$ is adopted.

(ii) Criteria for Biaxial Failure and Stress Reduction

Biaxial compressive failure may occur when stress becomes greater than σ_{ic} in Eq. (8) or E_i in Eq. (7) becomes little than zero. After the principal equivalent uniaxial strain reaches ε_{ic}, the stress in the direction is reduced by

$$\begin{cases} \Delta\sigma_i=-0.24E_0(\varepsilon_{iu}-\varepsilon_{ic})\geqq 0 & (4\varepsilon_{ic}\leqq\varepsilon_{iu}\leqq\varepsilon_{ic}) \\ \sigma_i=0 & (\varepsilon_{iu}<4\varepsilon_{ic}) \end{cases} \tag{12}$$

Biaxial strenght envelopes and stress reductions of the concrete model B are depicted in Figs. 4 and 5, respectively.

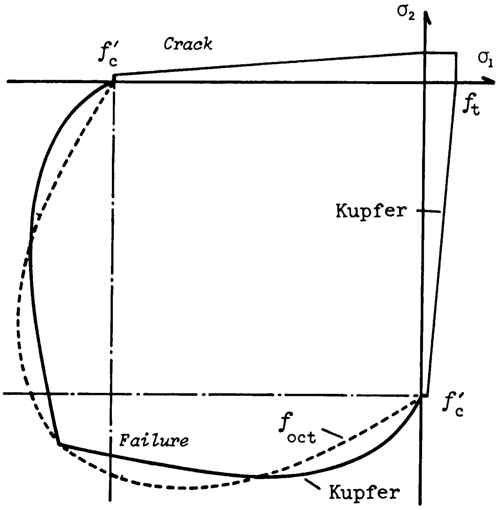

Fig. 4 Biaxial Strength for Concrete Model B

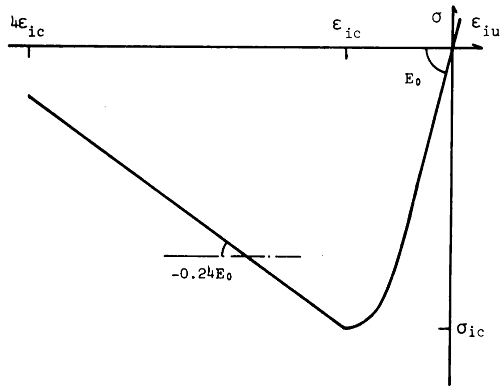

Fig. 5 Stress Reduction for Concrete B

2 − 2 Steel Bars

Reinforced steel is idealized as an elastoplastic strain hardening material. Then, stress-strain curves for the steel is shown in Fig. 6. No attempt to model bond slip is made in this study.

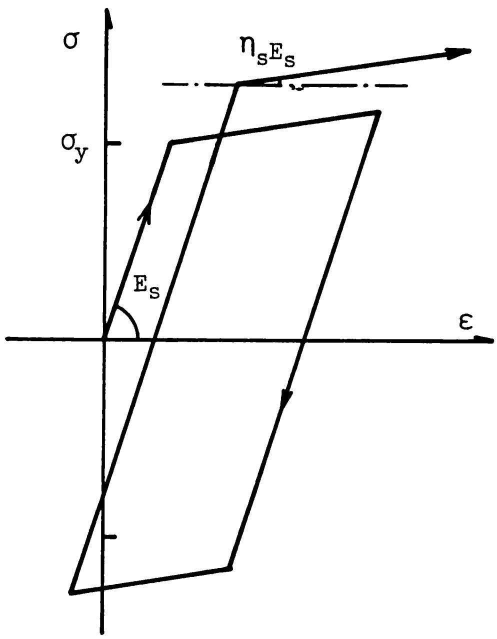

Fig. 6 Stress-Strain for Steel Bars

3 Finite Element Method

3 − 1 Finite Element Method

A flat triangular element with 15 degree-of-freedom is selected for this study. The element derives from incorporating a bending element, proposed by Zienkiewicz[12], and a constant strain membrane element. Evaluating finite deformations effects on the behavior of reinforced concrete slabs and shells, we include nonlinear terms with respect to the normal displacement.

3 − 2 Shape Functions of Triangular Plates

Setting each apex of a triangular element 1, 2 and 3, we determine x direction of element coordinates from 1 to 2, z direction as the direction of cross product $\overrightarrow{12}\times\overrightarrow{13}$, and y direction as x, y, z from right-handed rectangular Cartesian coordinates. Denoting displacements to x, y, z directions by u_i, v_i, w_i and rotations round x, y axes θ_{xi}, θ_{yi} at point i, we determine displacements u, v, w or u_1, u_2, u_3 corresponding to x, y, z directions.

$$\begin{Bmatrix} u_1 \\ u_2 \\ u_3 \end{Bmatrix} = \begin{Bmatrix} u \\ v \\ w \end{Bmatrix} = [\mathrm{N}_1\ \mathrm{N}_2\ \mathrm{N}_3] \begin{Bmatrix} \mathrm{d}_1^e \\ \mathrm{d}_2^e \\ \mathrm{d}_3^e \end{Bmatrix} = [\mathrm{N}]\{\mathrm{d}^e\} \tag{6}$$

where $\{\mathrm{d}_i^e\} = \{u_i,\ v_i,\ w_i,\ \theta_{xi},\ \theta_{yi}\}(i=1\sim3)$ and

$$[\mathrm{N}_1]^{\mathrm{T}} = \begin{bmatrix} \zeta_1 & 0 & 0 \\ 0 & \zeta_1 & 0 \\ 0 & 0 & \zeta_1(1+\zeta_1(\zeta_2+\zeta_3)-(\zeta_2^2+\zeta_3^2)) \\ 0 & 0 & -y_{12}\zeta_1\zeta_2(\zeta_1+\zeta_3/2)+y_{31}\zeta_3\zeta_1(\zeta_1+\zeta_2/2) \\ 0 & 0 & -x_{21}\zeta_1\zeta_2(\zeta_1+\zeta_3/2)+x_{13}\zeta_3\zeta_1(\zeta_1+\zeta_2/2) \end{bmatrix}$$

x_{21}, $y_{12}\cdots$ means x_2-x_1, $y_1-y_2\cdots$, when nodes 1, 2, 3 are expressed as (x_1 , y_1), (x_2 , y_2), (x_3 , y_3) in element coordinates, ζ_1, ζ_2, ζ_3 means area-coordinates, and $[\mathrm{N}_2]$, $[\mathrm{N}_3]$ are derived by interchanging subscript of 1, 2, 3, cyclically.

3 − 3 Members

We adopt a derivation where a neutral axis of member does not coincide with a neutral plane of a element included the member. Shape functions of members are assumed with cubic polynomial functions.

3 − 4 Stress-Strain relations

Examing geometrical nonlinearities effects, we include nonlinear terms of strains with respect to normal displacements. For two-dimensional elements the following strains and curvatures at neutral plane are used

$$\{\varepsilon^0\} = \begin{Bmatrix} \varepsilon_x^0 \\ \varepsilon_y^0 \\ \gamma_{xy}^0 \end{Bmatrix} = \begin{Bmatrix} u_{,x}+w_{,x}^2/2 \\ v_{,y}+w_{,y}^2/2 \\ u_{,y}+v_{,x}+w_{,x}w_{,y} \end{Bmatrix} = \begin{Bmatrix} u_{1,1}+u_{3,1}^2/2 \\ u_{2,2}+u_{3,2}^2/2 \\ u_{1,2}+u_{2,1}+u_{3,1}u_{3,2} \end{Bmatrix} \tag{7}$$

where subscripts x, y and 1, 2 denote a differential with respect to x, y, respectively,

$$\{\kappa\} = \begin{Bmatrix} \kappa_x \\ \kappa_y \\ \chi_{xy} \end{Bmatrix} = \begin{Bmatrix} w_{,xx} \\ w_{,yy} \\ 2w_{,xy} \end{Bmatrix} \tag{8}$$

Using Eqs. (7) and (8), strains at z from neutral plane $\{\varepsilon\}=\{\varepsilon_x, \ \varepsilon_y, \ \gamma_{xy}\}$ are given by

$$\{\varepsilon\}=\{\varepsilon^0\}-z\{\kappa\} \tag{9}$$

Assuming the infinitesimal displacements, we neglect nonlinear terms with respect to w in Eq. (7).

4 Incremental Equilibrium Equations and Unbalanced Forces

In order to perform analyses where geometrical and material nonlinearities are considered, we employ the incremental theory. The incremental equilibrium equations for three-dimentional elastic bodies are given by

$$\iiint_V [(\sigma_{ij}^{(0)}+\Delta\sigma_{ij})\delta(e_{ij}^{(0)}+\Delta e_{ij})-(\overline{P}_i^{(0)}+\overline{P}_i)\delta(u_i^{(0)}+\Delta u_i)]dV$$
$$-\iint_{S\sigma}(\overline{T}_i^{(0)}+\Delta\overline{T}_i)\delta(u_i^{(0)}+\Delta u_i)dS=0 \tag{10}$$

where $e_{ij}^{(0)}=(u_{i,j}^{(0)}+u_{j,i}^{(0)}+u_{k,i}^{(0)}u_{k,j}^{(0)})/2, \ \ e_{ij}^{(0)}+\Delta e_{ij}=$
$\{u_{i,j}^{(0)}+\Delta u_{i,j}+u_{j,i}^{(0)}+\Delta u_{j,i}+(u_{k,i}^{(0)}+\Delta u_{k,i})(u_{k,j}^{(0)}+\Delta u_{k,j})\}/2$. The values with $^{(0)}$ mean initial values and the values with Δ mean increments. Neglecting the incremental displacement product terms of higher order, we get the following equlibrium equations

$$\iiint_V\left[\Delta\sigma_{ij}\delta e_{ij}^*+\frac{1}{2}\sigma_{ij}^{(0)}\delta(\Delta u_{k,i}\Delta u_{k,j})-(\Delta\overline{P}_i\delta\Delta u_i+\overline{P}^{(0)}\delta\Delta u_i-\sigma_{ij}^{(0)}\delta e_{ij}^*)\right]dV$$
$$-\iint_{S\sigma}(\Delta\overline{T}_i+\overline{T}_i^{(0)})\delta\Delta u_i dS=0 \tag{11}$$

where $e_{ij}^*=(\Delta u_{i,j}+\Delta u_{j,i}+u_{k,i}^{(0)}\Delta u_{k,j}+u_{k,j}^{(0)}\Delta u_{k,i})/2$

In order to apply Eq. (11) to slabs and shells, we transform the expression. Expressing argument angle θ between principal stress or strain directions and the element coordinates, we have stress-strain matrix $[D_{xy}]$ defined in the element coordinates

$$[D_{xy}]=[R]^T[D_{12}^*][R] \tag{12}$$

where $[D_{12}^*]$ is given by Eq. (1) or (11), and

$$\{R\}=\begin{bmatrix} \cos^2\theta & \sin^2\theta & \sin 2\theta/2 \\ \sin^2\theta & \cos^2\theta & -\sin 2\theta/2 \\ -\sin 2\theta & \sin 2\theta & \cos 2\theta \end{bmatrix}$$

Using incremental displacement vectors $\{\Delta d^e\}$ and Eq. (12), we get the expression of incremental stresses

$$\begin{Bmatrix} \Delta\sigma_{11} \\ \Delta\sigma_{22} \\ \Delta\sigma_{12} \end{Bmatrix} = \begin{Bmatrix} \Delta\sigma_x \\ \Delta\sigma_y \\ \Delta\tau_{xy} \end{Bmatrix} =[D_{xy}][B_1(w^{(0)})]\{\Delta d^e\} \tag{13}$$

where $[B_1]\{\Delta d^e\}$ is a matrix form of the following

$$[B_1]\{\Delta d^e\}= \begin{Bmatrix} \Delta u_{,x}+w_{,x}^{(0)}\Delta w_{,x}-z\Delta w_{,xx} \\ \Delta v_{,y}+w_{,y}^{(0)}\Delta w_{,y}-z\Delta w_{,yy} \\ \Delta u_{,y}+\Delta v_{,x}+w_{,x}^{(0)}\Delta w_{,y}+w_{,y}^{(0)}\Delta w_{,x}-2z\Delta w_{,xy} \end{Bmatrix}$$

Considering nonlinear strains terms with respect to the normal displacement w, we can express the second term in Eq. (11)

$$2\sigma_{ij}^{(0)}\delta(\Delta u_{k,i}\Delta u_{k,j})=\sigma_x^{(0)}\Delta w_{,x}\delta\Delta w_{,x}+\sigma_y^{(0)}\Delta w_{,y}\delta\Delta w_{,x}+\tau_{xy}^{(0)}(\Delta w_{,x}\delta\Delta w_{,y}+\Delta w_{,y}\delta\Delta w_{,x})$$
$$=\delta\{\Delta d^e\}^T[B_2]^T[S][B_2]\{\Delta d^e\} \tag{14}$$

where $[S]=\begin{bmatrix} \sigma_x^{(0)} & \tau_{xy}^{(0)}/2 \\ \tau_{xy}^{(0)}/2 & \sigma_y^{(0)} \end{bmatrix}$, $[B_2]\{\Delta d^e\}=\begin{Bmatrix} \Delta w_{,x} \\ \Delta w_{,y} \end{Bmatrix}$

Substituting Eqs. (13) and (14) into Eq. (11), we have

$$\delta\{\Delta d^e\}^T\iiint_V([B_1]^T[D_{xy}][B_1]+[B_2]^T[S][B_2])dV\{\Delta d^e\}-\delta\{\Delta d^e\}^T\{\Delta f\}=0 \tag{15}$$

where $\delta\{\Delta d^e\}^T\{f\}=(\iiint_V \Delta\bar{P}_i\delta\Delta u_i dV+\iint_{S\sigma}\Delta\bar{T}_i\delta\Delta u_i dS)$

$$+(\iiint_V(\bar{P}_i^{(0)}\delta\Delta u_i-\delta\{\Delta d^e\}^T[B_1]^T\{\sigma_x^{(0)}\sigma_y^{(0)}\tau_{xy}^{(0)}\})dV+\iint_{S\sigma}\bar{T}_i^{(0)}\delta u_i dS) \tag{15-a}$$

The first term in Eq. (15-a) corresponds to incremental external forces and the second term means unbalanced forces caused by neglecting the incremental product terms of higher order, stress reductions by cracking, yielding and unloadings.

Dividing a triangular element in similar m_j subelements and m_e layers, we evaluate the volume integral in Eq. (15) in the subvolumes $m_j\times m_e$. Here we employ $m_j=4$ and $m_e=8$.

5 Numerical Analyses

Associating two assumptions about deformations where one assumes infinitesmal displacements and the other includes finite displacements, and two concrete models given in 2, we construct 4 solving methods and analyze 4 reinforced concrete slab specimens, US−1 and US−2 tested by Higashi and Komori[3], A slab tested by Dobashi and Ueda[21], and the corner supported slab tested by Jofriet and McNeice.[2] They are depicted in Table 1.

Table. 1　Data for Model Slabs

	Plan Size	Edge Beam Size H×W	Thickness of Slab	Steel Ratio p_t (%)	Steel Position from Top Surface	Number of Loading Point
US−1	70×70(cm)	20×40(cm)	2.9(cm)	1.22	1.45(cm)	16
US−2	70×70(cm)	20×20(cm)	3.3(cm)	1.22	1.65(cm)	16
A slab	120×120(cm)	Min. 60×80(cm) Max. 60×130(cm)	4.97(cm)	0.32	2.80(cm)	9
McNeice	36×36(inch)		1.75(inch)	0.85	1.31(inch)	1

Having large size edge beams, US−1 and A slab are idealized as slabs with clamped edges. Setting material properties depicted in Tables 2 and 3, we solve them and express load-deflection curves in Figs 7 and 9, respectively, where a dot-dash-line indicates the experimental curve, a solid line indicates a solution obtained by considering finite displacements with concrete model A, a dotted line indicates a solution obtained by considering finite displacements with concrete model B, a solid line with ○ indicates a solution obtained by assuming infinitesimal displacements with concrete model A, and a dotted line with ○ indicates a solution obtained by assuming infinitesimal displacements with concrete model B, which are used in all other figures in this paper. And a dot-dot-dash-line with ● indicates the result obtained by Dobashi[21]. Computed load-compressive membrane stress N_x evaluated at centroid of C element of specimens US−1 and A slab are presented in Figs. 8 and 10, respectively.

In US−2, edge beams are also modeled with finite elements. Analyzed load-deflection curves and load-N_x curves are presented in Figs. 11 and 12.

Except ultimate stages, the solving methods assuming infinitesimal displacements give a similar curve and the solving methods considering finite displacement give a similar curve whether

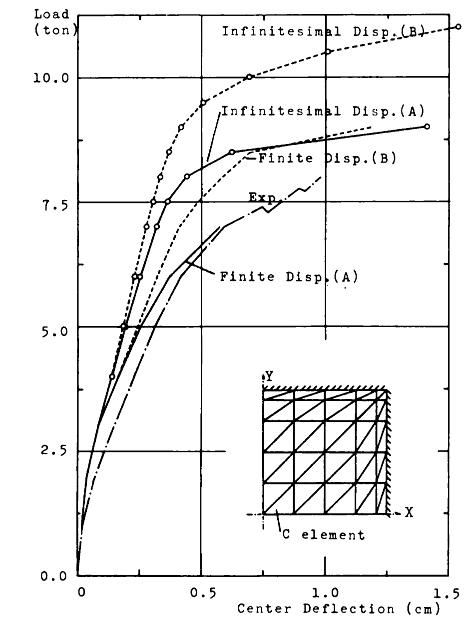

Fig. 7 Load vs Center Deflection Curves (US-1)

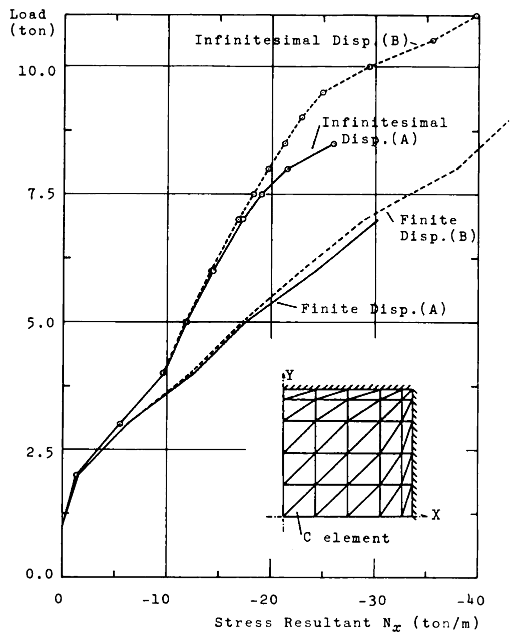

Fig. 8 Load vs Nx Curves (US-1)

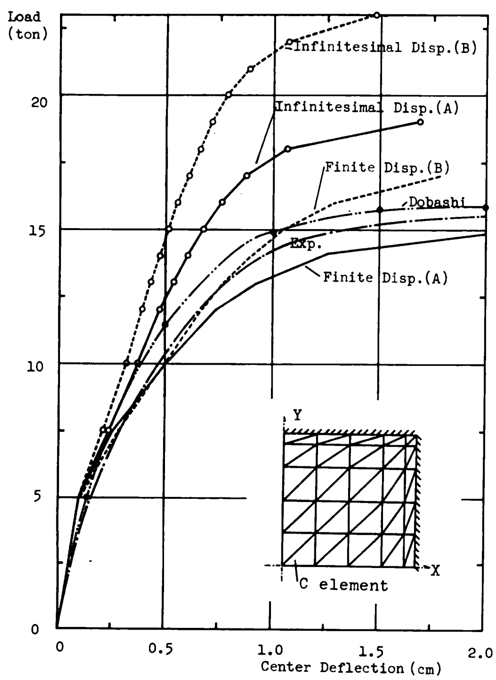

Fig. 9 Load vs Center Deflection Curves (A slab)

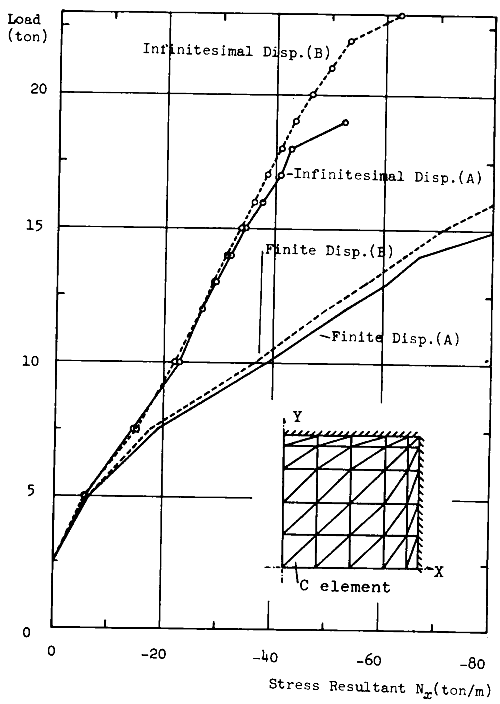

Fig. 10 Load vs Nx Curves (A slab)

concrete model A or B is employed. But there are decided differences between them. The solutions obtained by considering finite displacements give match resuls with experiments. And concrete model B gives larger ultimate loads than concrete model A. Then, comparing the results of US−1 and US−2 being appoximately the same size slabs, US−1 had larger compressive membrane stress resultant than US−2, but US−1 gave a smaller ultimate load and showed lesser

Tablel. 2　Material Properties for Concrete Model A

	E_c	f'_c	ε_{cu} (%)	Poisson Ratio ν	ε_t	ε_1	ε_2	η_1	η_2
US-1	2.1×10^5(kg/cm²)	-220(kg/cm²)	-0.21	0.15	0.0001	-0.000524	-0.001465	0.558	0.0465
US-2	2.0×10^5(kg/cm²)	-230(kg/cm²)	-0.21	0.15	0.0001	-0.000575	-0.001605	0.558	0.0465
A slab	2.1×10^5(kg/cm²)	-240(kg/cm²)	-0.21	0.20	0.00009	-0.000571	-0.001595	0.558	0.0465
McNeice	4.15×10^6(psi)	-5500(psi)	-0.21	0.15	0.00012	-0.000663	-0.00185	0.558	0.0465

Tablel. 3　Material Properties for Concrete Model A and Steel Bars

	E_o	f'_c	ε_{cu} (%)	Poisson Ratio ν	f'_t	E_s	σ_y	η_s
US−1	2.1×10^5(kg/cm²)	-220(kg/cm²)	-0.21	0.2	21(kg/cm²)	2.09×10^6(kg/cm²)	2430(kg/cm²)	0.01
US−2	2.0×10^5(kg/cm²)	-230(kg/cm²)	-0.21	0.2	20(kg/cm²)	2.09×10^6(kg/cm²)	2430(kg/cm²)	0.01
A slab	2.5×10^5(kg/cm²)	-240(kg/cm²)	-0.21	0.2	19.2(kg/cm²)	2.1×10^6(kg/cm²)	4500(kg/cm²)	0.01
McNeice	4.15×10^6(psi)	-5500(psi)	-0.21	0.2	480(psi)	29×10^6(psi)	50000(psi)	0.01

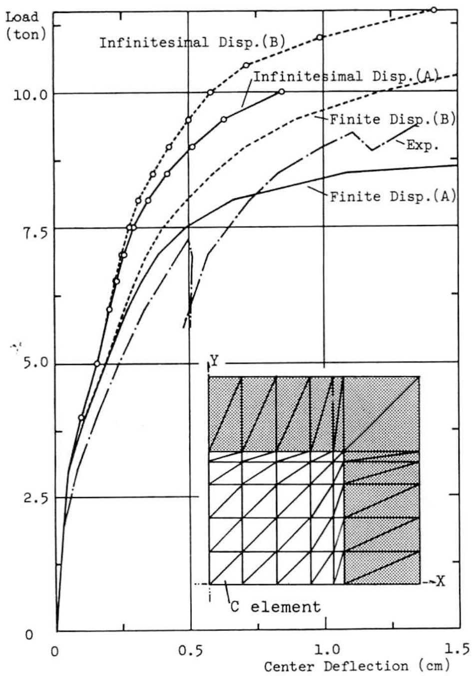

Fig. 11　Load vs Center Deflection Curves (US-2)

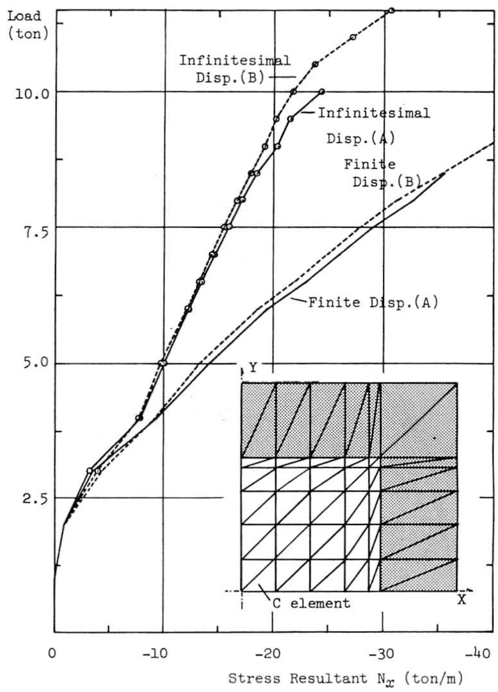

Fig. 12　Losd vs Nx Curves (US− 2)

ductile behaviors than US−2. The phenomenon may express that the geometrical nonlinearities stimulated by the large membrane stress resultants have considerable effects on the behaviors of the slabs with inplane constraint.

Next, we employ a slab supported at 4 corner points, and examine effects of finite displacements on reinforced concrete slabs with inplane inconstraint. Applying foregoing 4 solving methods, we analyze the slab under roller and pin supports, and show results in Figs. 13 and 14,

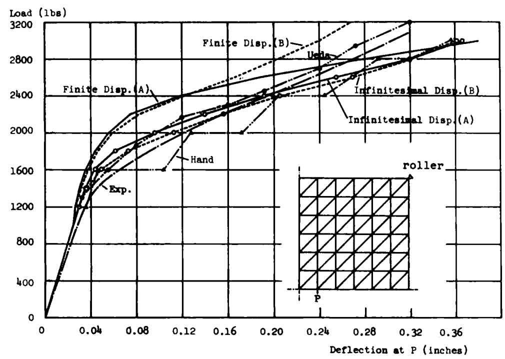

Fig. 13 Load vs Center Deflection Curves for McNeice'(roller)

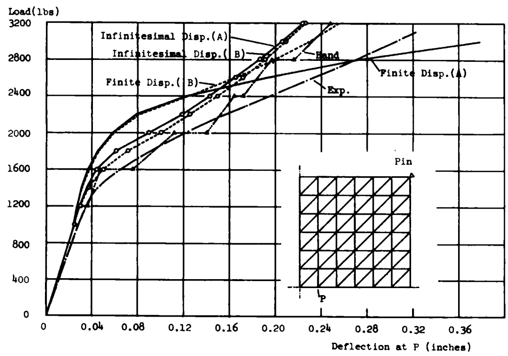

Fig. 14 Load vs Center Deflection Curves for McNeice'(pin)

respectively. In both figures a dash-dot-dot-line with ▲ indicates the results reported by Hand[3], and in Fig. 13 a dash-dot-dot-line with ● indicates the results reported by Ueda[18]. The solutions obtained by assuming infinitesimal displacements give a similar behavior with Hand and Ueda. However, the solutions obtained by considering finite displacements show increase of stiffness just after elastic regions caused by geometrical nonlinearities.

6 Conclusions

1. The compressive membrane stress resultants, produced in elastic-plastic stages of reinforced concrete slabs with inplane constraint, let stimulate geometrical nonlinearities and have considarable influences on load-deflection behavior of them.

1. For slabs with massive edge beams, the nonlinearities make behave with lack of ductility. And ultimate loads for the slabs may become smaller than that for the same size slabs with lesser edge beams.

1. Increase of stiffness just after elastic stages is observed in load-deflection curves of a corner supported slab, which is caused by geometrical nonlinearities.

REFERENCES

1) H. B. Kupfer and K. H. Gerstle, "Behavior of Concrete under Biaxial Stresses," ASCE, Vol. 99, EM4, 1973

2) J. C. Jofriet and G. M. McNeice, "Finite Element Analysis of Reinforced Concrete Slab," ASCE, Vol. 97, ST3, 1971

3) F. R. Hand, D. A. Pecknold and W. C. Schnobrich, "Nonlinear Layered Anaylsis of RC Plates and Shells, "ASCE, Vol. 99, ST 7, 1973

4) M.K. Wanchoo and G.W. May, "Cracking Analysis of Reinforced Concrete Plates," ASCE, Vol. 101, ST 1, 1975

5) C.S. Lin and A.C. Scordelis, "Nonlinear Analysis of RC Shells of General Form, "ASCE, Vol. 101, ST3, 1975

6), D. Darwin and D.A. Pecknold, "Analysis of RC Shear Panels under Cyclic Loading," ASCE, Vol. 102, ST2, 1976

7) D. Darwin and D.A. Pecknold, "Nonlinear Biaxial Stress-Strain Law for Concrete,"ASCE, Vol. 103, EM2, 1977

8) P. Desayi and A.B. Kulkarni, "Load-Deflection Behavior of Restrained R/C Slabs," ASCE, Vol. 103, ST2, 1977

9) F.K. Bashur and D. Darwin, "Nonlinear Model for Reinforced Concrete Slabs," ASCE, Vol. 104, ST1, 1978

10) Timoshenko and Gere, "Theory of Elastic Stability," McGraw-Hill

11) K. Washizu, "Variational Method in Elasticity & Plasticity," Third Edition Pergamon Press

12) O.C. Zienkiewicz, "The Finite Element Method," McGraw-Hill

13) 東，小森"等分布荷重を受ける鉄筋コンクリート正方形スラブの終局耐力に関する実験的研究"建論第140号昭和42年

14) 磯畑"有限要素法によるコンクリート構造物の2次元弾塑性解析"建論第189号，昭和46年

15) 岡島"2軸応力を受けるコンクリートの破壊ひずみ"材料第22巻第232号，昭和48年

16) 小森"鉄筋コンクリートスラブの耐力とたわみ性状に関する研究"建論第269，285，311号

17) 内山，上田，土橋"鉄筋コンクリート床版の弾塑性解析"建論第276号，昭和54年

18) 上田，土橋"鉄筋コンクリート床版の非線形解析"建論283号，昭和54年

19) 建築学会構造標準委員会"鉄筋コンクリート終局強度設計に関する資料"建築雑誌Vol. 94, No. 1145, No. 1146, 昭和54年

20) 野口"有限要素法による鉄筋コンクリートの非線形解析"建論252号，昭和52年

21) 土橋，上田，"周辺を拘束したRC床版の圧縮膜効果について"建論第296号昭和55年

22) 藤田，磯畑，川股，坪井"有限要素法による鉄筋コンクリートシェルの弾塑性解析"建築大会昭和55年

23) 上田，瀬谷，毛井"鉄筋コンクリートシェル構造物の有限要素解析"建築大会昭和58年

24) 玉井，塩見，近藤，末岡，花井"新しい離散化手法によるRC床版の弾塑性解析"建築大会昭和59年

25) 皆川"幾何学的非線形性を考慮した鉄筋コンクリート造スラブ及びシェルの弾塑性解析"建築学会九州支部昭和60年